Rotating Wall Technique and Centrifugal Separation

François Anderegg
University of California San Diego, Physics Dept. 0319,
La Jolla CA 92093, USA
fanderegg@UCSD.edu

This chapter describes the "rotating wall" technique which enables essentially unlimited confinement time of 10^9 to 10^{10} charged particles in a Penning trap. The applied rotating wall electric field provides a positive torque that counteract background drags, resulting in radial compression or steady state confinement in near-thermal equilibrium states.
The last part of the chapter discuss centrifugal separation of rotating multi-species non-neutral plasma. Separation occurs when the centrifugal energy is larger than the mixing due to thermal energy.

1. Basic Physics Idea

Let's consider a non-neutral plasma contained in a Penning-Malmberg trap as shown on figure 1. The trap consist of a series of cylindrical electrodes carefully aligned with the magnetic field $\boldsymbol{B} = -B\hat{z}$. Longitudinal confinement is produced by potentials V applied to the end electrodes, and radial confinement is produced by the magnetic field. For simplicity, let's assume

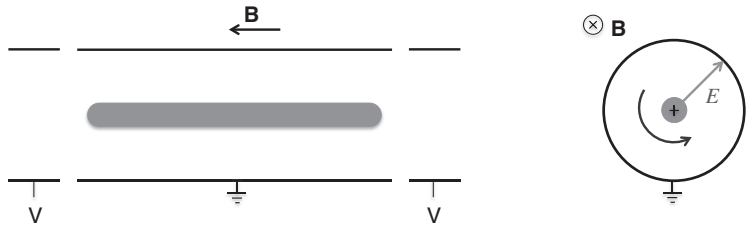

Fig. 1. Penning-Malmberg trap.

that the plasma consist of positive charges, so our choice of $\boldsymbol{B}$ direction will make all rotation frequencies and velocities positive.

The charges produce a radial electric field pointing to the wall, creating an azimuthal $\boldsymbol{E}\times\boldsymbol{B}$ drift of the particles $v_\theta = E_r/B$, resulting in a rotation frequency:

$$f_E = \frac{v_\theta}{2\pi r} = \frac{E_r}{B2\pi r} \ . \tag{1}$$

The electric field satisfies Gauss' law:

$$\nabla \cdot \boldsymbol{E} = \frac{nq}{\epsilon_0} \ , \tag{2}$$

and in cylindrical coordinates, the radial component is:

$$\frac{1}{r}\frac{\partial}{\partial r}(rE_r) = \frac{nq}{\epsilon_0} \ . \tag{3}$$

Multiplying by r and integrating gives:

$$rE_r = \frac{q}{\epsilon_0}\int_0^r n(r')r'dr' \ . \tag{4}$$

For a radially uniform density:

$$E_r = \frac{q}{\epsilon_0 r} = \frac{1}{2}r^2 n = \frac{rnq}{2\epsilon_0} \ , \tag{5}$$

therefore

$$f_E = \frac{nq}{4\pi\epsilon_0 B} \ . \tag{6}$$

One sees that for a uniform density plasma the rotation is constant out to the plasma edge r_p ; that is the plasma is rotating as a rigid rotor, at a rate proportional to the density n.

Non-neutral plasma have extraordinary confinement properties,[1] in particular in a azimuthally symmetric system the plasma angular momentum P_θ is conserved

$$P_\theta = \sum_j \left(mv_{\theta j} + qA_\theta r_j\right) \ , \tag{7}$$

with $A_\theta = B\,r/2$ for a uniform magnetic field. The first term is the mechanical angular momentum and the second is the canonical angular momentum.

For large magnetic field the canonical angular momentum term dominates and

$$P_\theta \cong \sum_j \frac{qBr_j^2}{2} \tag{8a}$$

$$P_\theta^T \cong \sum_j \frac{qB}{2}(r_j^2 - R_W^2)\ , \tag{8b}$$

where the sum on j is over all the particles in the trap. The P_θ^T of equation 8b explicitly includes both the plasma charges and an equal number of image charges located at R_W and may be seen as more intuitive. Note that equation 8b is valid for cylindrical trap with uniform wall radius, and reflects the fact that the magnitude of the total angular momentum is minimum when all particles have been lost at the wall.

Therefore if one particle move outward increasing its r_j, other particles have to move inwards. Consequently in theory, non-neutral plasmas relax towards a confined thermal equilibrium state as viewed in a frame rotating at rate f_E.

In reality, perfect symmetry is never realized in the laboratory. Residual gas, magnetic field asymmetries, and electrodes imperfections create drags on the rotating plasma, reducing its rotation rate and therefore decreasing its density and its angular momentum.

There are several methods to add angular momentum to the particles of a Penning trap:

- In the single particle regime, a sideband technique known as "*axialisation*" couples the magnetron motion to an "other" motion in the trap (either cyclotron or axial). The "other" motion is damped, either by laser cooling or by a resonant circuit, resulting in a radial compression of the particle density. The axialisation technique works in the single particle regime, but not in the plasma regime where the Debye length λ_D is smaller than the plasma radius r_p. This axialisation technique has been presented in detail during the winter school and the chapter written by R. Thompson in this volume covers the subject.
- The radiation pressure of a laser has been successfully used to torque on the plasma and increase its density.[2]
- In principle rotating the entire trap at the plasma rotation frequency f_E would alleviate the drag on the plasma, but this is rather impractical since non-neutral plasmas typically rotate at 1kHz $\leqslant f_E \leqslant$100MHz. No

macroscopic objects can rotate at these rates due to the limitation of material strength. A more practical solution is to apply a time-varying potential to azimuthally sectored electrode, at frequencies f_{RW}.

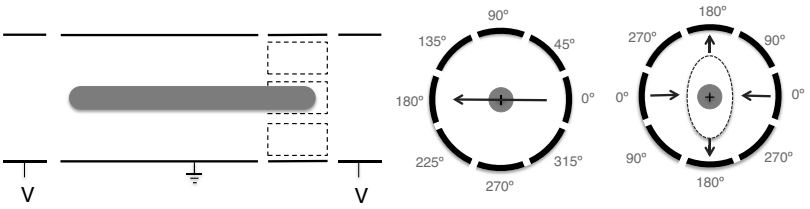

Fig. 2. Segmented electrode to apply "rotating wall" perturbation with dipole $m_\theta = 1$ and quadrupole drive $m_\theta = 2$.

Figure 2 shows schematically an azimuthally segmented electrode for applying a "rotating wall" perturbation. The time dependent potential applied to each azimuthal sector is:

$$\begin{aligned} &\phi_j(\theta, t) = A_{RW} \cos\left[m_\theta \left(\theta_j - 2\pi f_{RW} t\right)\right] \ , \\ &\theta_j - \tfrac{\Delta\theta}{2} < \theta < \theta_j + \tfrac{\Delta\theta}{2} \ ; \end{aligned} \tag{9}$$

here m_θ=1 represents a dipole drive and m_θ=2 a quadruple drive. The signal applied to each sector is a sine wave with a phase shifted by θ_j. Inside the trap, a charged particle "*sees*" a rotating electric field.

The fundamental concept of a rotating electric field is simple but due to the finite size of sectored electrodes, unwanted spatial harmonics can be significant. An extreme example is applying a quadrupole drive with only four electrodes, where the amplitude of the backward rotating electric field (m_θ=-2) is as large as the forward one ($A_{m_\theta=-2}/A_{m_\theta=2} = 1$). One should note that the plasma may still couple to one direction preferentially, since the rotating perturbation is Doppler shifted in the plasma rotating frame. Using eight sectors significantly improves the quality of the drive. Here the strongest backward rotating component is m_θ=-6, ($A_{m_\theta=-6}/A_{m_\theta=2} \cong 2/3$) that is the useful m_θ=2 component is about 60% of the signal compared to about 40% m_θ=-6 rotating backward.

1.1. *Torque Balance*

The plasma is in equilibrium when the sum of all the torques applied to the plasma equals zero. Ambient, lab-frame effects such as collisions with

residual gas particles or an asymmetric $\boldsymbol{B}$ field will exert a "drag" on the rotating plasma. In contrast a rotating wall with $f_{RW} > f_E$ will "spin-up" the plasma. A drag decreases the magnitude of P_θ^T and increases $< r_j^2 >$, whereas spinning-up increases the magnitude of P_θ^T and decreases $< r_j^2 >$. This can be proven formally using thermodynamics argument.[3]

Steady state is achieved when

$$|\tau_{RW}| = |\tau_{ambient}| \,, \tag{10}$$

and the compression of the plasma happens when

$$|\tau_{RW}| > |\tau_{ambient}| \,. \tag{11}$$

In principle any electric field rotating faster than the plasma will torque on a plasma and compress it; but Debye shielding may render the rotating wall torque too small to be useful. The rotating wall field can be greatly enhanced by a plasma wave resonance, and working in the vicinity of azimuthally rotating plasma modes has been generally successful. It is often easier to couple to these rotating modes from the end of the plasma column.

Any radially expanding plasma is necessarily releasing electrostatic energy, resulting in plasma heating. The minimum heating that the plasma will have in the presence of an "*ideal*" rotating wall balancing ambient torques will be:

$$2\pi f_{RW} \tau_{RW} = 2\pi f_E \tau_{ambient} \tag{12}$$

In general, the heating will be larger due to the presence of unwanted spatial harmonics and imperfection in the rotating wall drive. Typically the unwanted spatial harmonics are reduced by increasing the number of azimuthal sectors, but no systematic experiment have been performed yet.

At high temperatures, plasma modes are damped and plasma are less collisional; both effects are reducing coupling to the rotating wall electric field. Therefore to successfully implement the rotating wall technique, a cooling sufficient to balance the unwanted heating is necessary.

1.2. *Typical Form of Cooling Used for Rotating Wall*

1.2.1. *Cyclotron radiation*

An accelerated charge q radiates energy at a rate given by the Larmor formula:

$$\frac{dE}{dt} = \frac{q^2 a^2}{6\pi\epsilon_0 c^3} \,. \tag{13}$$

For a charged particle gyrating in a magnetic field, the acceleration is $a_\perp = \Omega_c v_\perp$ and energy is $E_\perp = \frac{1}{2}mv_\perp^2$ resulting in:

$$\frac{dE_\perp}{dt} = \frac{q^2\Omega_c^2 E_\perp}{3\pi\epsilon_0 mc^3} \,. \tag{14}$$

Averaging the above equation over a Maxwellian distribution yields:[4,5]

$$\frac{dT_\perp}{dt} = \frac{-3T_\perp}{2\tau_r} \tag{15}$$

with radiation time τ_r given by

$$\tau_r = \frac{-3T_\perp}{2\dot{T_\perp}} = \frac{3}{2}\frac{T_\perp 3\pi\epsilon_0 mc^3}{q^2\Omega_c^2 T_\perp} = \frac{9}{2}\frac{\pi\epsilon_0 m^3 c^3}{q^4 B^2} \,. \tag{16}$$

One sees that the radiation time is short for light particles in a large magnetic field; for electrons (or positrons):

$$\tau_r = \frac{3.86 \text{ sec}}{B^2_{\text{Tesla}}} \,. \tag{17}$$

In contrast ions are too massive to be cooled by cyclotron radiation in any practical trap magnetic field.

1.2.2. *Collisions with residual gas particles*

Effective ion cooling can be achieved from collisions with residual gas particles at rate ν_{iN}. The gas is at temperature T_N and the cooling rate is:

$$\dot{T} \cong \nu_{iN}(T - T_N) \tag{18}$$

One sees that if the difference of temperature in between the gas and the plasma is large, then collisions with background gas is effective. The ion-neutral collision rate ν_{iN} is typically of the order of 10^{-2}sec^{-1}. For example, magnesium ions colliding with H_2 through dipole interactions, one obtains:

$$\nu_{iN} \cong 0.019\text{sec}^{-1}\left(\frac{P_N}{10^{-9}\text{ mbar}}\right) \qquad \left(\text{Mg}^+\text{on}\text{H}_2\right) \tag{19}$$

Succesful cooling of positron, has also been achieved using vibrational modes of large gas molecules.[6]

1.2.3. *Laser cooling*

This technique has been presented in detail during the winter school and the chapter written by C. Champenois in this volume covers the subject. Laser cooling is effective to cool ions, but only a few kind of ions can be laser cooled since closed two level system is preferred.

Sympathetic cooling has been successfully used to cool other ion through collision with laser cooled ion,[7] or to cool antiproton with electron that are cooled by cyclotron radiation.[8]

2. Results from Various Experiments

The rotating wall technique has been implemented on numerous experiments. Here I will briefly review results from 3 experiments. The first one is the original demonstration of the rotating wall technique, demonstrating the importance of plasma modes in the coupling. The second shows the "strong drive regime", and the third experiment demonstrates that a crystallized plasma can phase-locked its rotation to the rotating wall drive.

2.1. *Rotating Wall Coupled Through Plasma Modes*

Experiment in Penning-Malmberg traps containing about 10^9 magnesium ions or 3×10^9 electrons have demonstrated that a rotation wall perturbation can control the plasma density and radius; and that the confinement time of the particles is essentially "infinite" (weeks).[9] For electron experiments with a magnetic field of 4 Tesla, cyclotron cooling is rapid with cooling time $\tau_r \sim 0.24$sec. For the data presented in this section, ions plasma are cooled by weak collisions with residual gas particles giving cooling time $\tau \sim 20.$sec.

Both dipole (m_θ=1) and quadruple (m_θ=2) rotating wall drive produce significant plasma compression for both electrons and ions. The experimental arrangement used a rotating wall perturbation applied to the end of the plasma column as shown on figure 2. Density profiles for both electron and ion plasma are shown on figure 3a. The electron density is measured with a destructive plasma dump on a moveable collimator plate with a small hole. The charge passing through the small hole is measured by a Faraday cup resulting in a line integrated density. The density is obtained by dividing the line integrated density by the plasma length.

A low density plasma (A) is compressed by sweeping up the rotating wall frequency slowly into profile (B) and (C). The ion density profiles measured with Laser Induced Fluorescence are shown on the upper frame.

These profiles are steady state and confined for periods of weeks. One should note that ion plasmas that are confined for a long time exhibit slow chemical reactions even at ultra high vacuum, with residual background gas (mainly H_2) converting metallic ion into metal hydride ions.

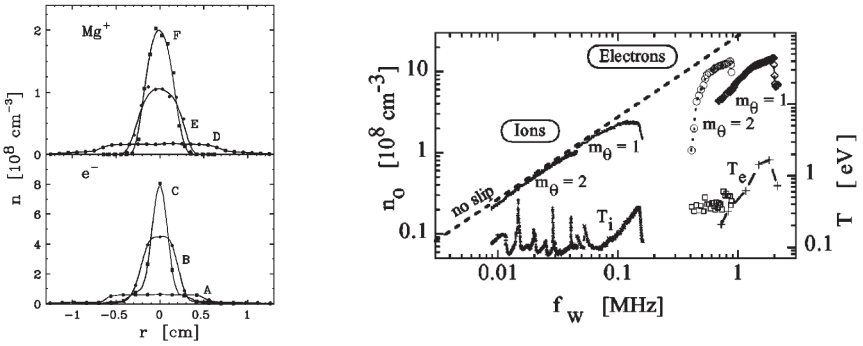

Fig. 3. Left) Electron and ion density profiles. Right) Density and temperature during rotating wall frequency sweep.

Figure 3b shows the central plasma density plotted versus the rotating wall frequency. As the frequency is ramped up, the plasma density increases and the rotation frequency f_E of equation 6 increases. The plasma rotation frequency is always lower than the rotating wall frequency ($f_{RW} > f_E$) and therefore some "slip" is present. The maximum ion density achieved in this experiment was 13% of the Brillouin density (i.e. maximum stable density in a Penning trap). As the density increases, the background drag increases as $\sim n_0^2$ while the rotating wall torque remain constant, so the slip increases. More heating is generated and the rotating wall coupling decreases, leading to a abrupt reduction of the density in the trap.

Also, the plasma temperature shows spikes each time the rotating wall drive imperfections excite a longitudinal plasma mode. Here the longitudinal plasma modes are detrimental to the rotating wall coupling. Care should be taken to rapidly change the rotating wall frequency when one such mode is encountered, otherwise the control of the plasma density may be lost since the coupling decreases as the temperature increase.

Figure 4 demonstrates that the coupling of the rotating wall to the plasma is much larger in the vicinity of azimuthal (rotating) plasma modes, for both $m_\theta = 1$ and $m_\theta = 2$. Here the electron plasma profile B of figure 3a is in equilibrium with the rotating wall at f_{RW}=0.5 MHz, then f_{RW}

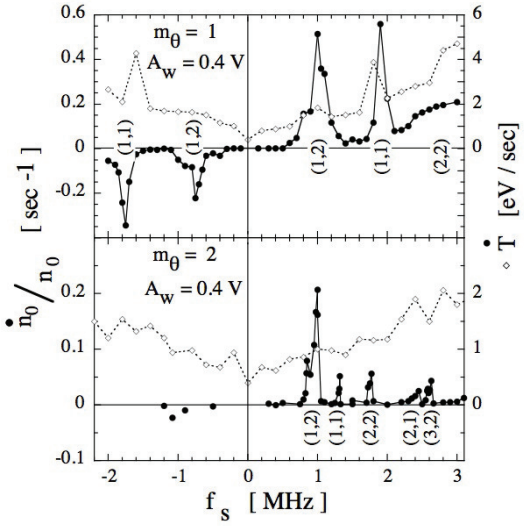

Fig. 4. Compression rate versus rotating wall frequency for $m_\theta = 1$ and $m_\theta = 2$ drives.

is changed and the compression rate is measured at $r = 0$. When the rotating wall frequency is close to an azimuthal plasma mode characterized by (m_z, m_r), the compression rate is significantly larger. When the rotating wall is phased so as to rotate backwards (labeled as negative frequencies on figure 4, rapid expansion is observed in the vicinity of backward traveling modes.

Compression peaks are broadened and their amplitude is reduced due to Landau damping when the temperature gets too high. Depending on the plasma geometry and particles masses, compression peaks due to plasma mode can be very broad and appear continuous.

On figure 4 one sees that the heating rate increases as f_{RW} increases due to increased slip rate.

2.2. *Strong Drive regime*

This technique relies on a large amplitude drive and seems to be less sensitive to plasma modes, when the cooling rate is large enough and the background drag small enough. The geometry of this experiment is similar to the canonical Penning-Malmberg trap, with a rotating wall applied at the end of the plasma column as show on figure 2. Typically $\sim 10^9$ electrons are confined in a magnetic field of $B = 5.\mathrm{T}$ resulting in a strong cyclotron

radiation with a cooling time $\tau_r = 0.15$ sec. A dipole ($m_\theta = 1$) drive is applied at a fixed frequency.[10]

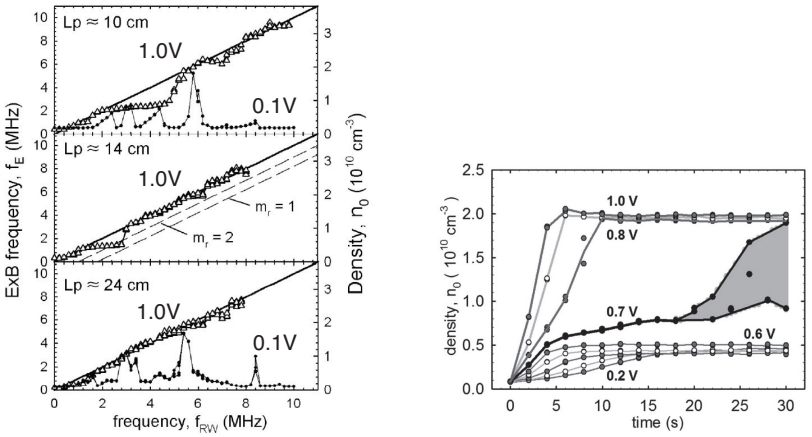

Fig. 5. a)Weak (0.1V) and strong drive(1.0V), b) Density below and above critical amplitude (0.7V).

Two distinct plasma responses are observed depending on the strength of the rotating wall drive. At low amplitude (0.1V), compression is observed only at discrete rotating wall frequencies as shown on figure 5a, due to plasma modes couplings. At large amplitude (1.0V) compression is observed over a wide range of frequencies and no significant slip is observed. In this experiment, the rotation frequency is inferred from a density measurement, and no direct rotation frequency measurement is performed. At large amplitude the central frame of figure 5a suggest that the plasma is rotating faster than the rotating mode frequencies indicted by dashed lines.

Also a bifurcation behavior is observed as the amplitude of the drive exceeds a critical strength of 0.7V as shown in figure 5b, the plasma density rapidly reaches $n = 2 \times 10^{10}\text{cm}^{-3}$.

Here the increased cyclotron cooling and the low background transport is what allow this new regime to be observed.

2.3. *Phased-Locked Rotating Crystal*

Beryllium ions contained in a Penning trap are laser cooled to $T < 10$mK ($\sim 10^{-6}$eV). The plasma consists of $10^2 < N < 10^6$ ions, and is strongly coupled, since the potential energy between neighboring ions is larger that

the ion thermal energy. The rotating wall perturbation is applied uniformly across the axial extend of the plasma with 2 sets of azimuthally segmented electrodes (the compensation electrodes). Plasma compression is observed with both m_θ=1 and m_θ=2 drives.[11]

Theoretically, the dipole field (m_θ=1) can not control the plasma rotation of a single-species plasma in a quadratic trap. This is because it only causes a center-of-mass orbital motion about the trap axis and is thus decoupled from the internal plasma rotation. Experimentally the dipole field (m_θ=1) works in the presence of impurities ions, while the quadrupole field (m_θ=2) always works. The NIST trap is shown schematically in figure 6a.

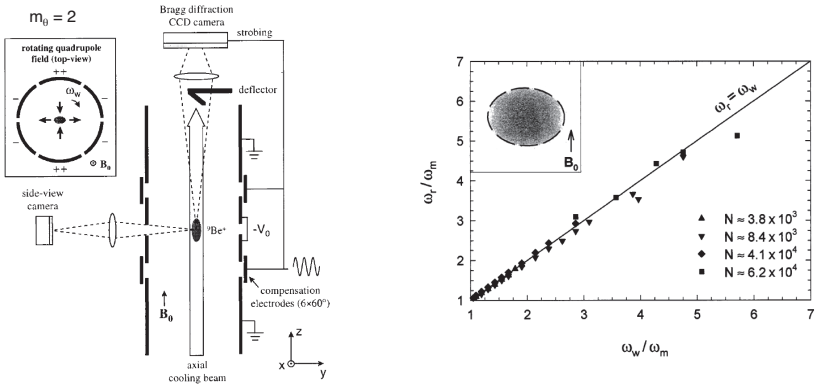

Fig. 6. a) NIST trap for ion crystal b)Plasma rotation controlled with rotating wall frequency.

Figure 6b shows the plasma rotation frequency inferred from the measured plasma aspect ratio. The plasma rotation frequency increases linearly with the applied rotating wall frequency, in both weakly and strongly coupled plasmas.

For a more accurate determination of the rotation rate, the time dependance of Bragg-scattered light from the rotating crystal has been detected by strobing the camera. Without strobing, figure 7a show the time averaged diffraction pattern of concentric ring because of the plasma rotation about the axial laser beam. With strobing, figure 7b shows a time-resolved pattern accumulated over 10^6 rotations. The well-defined rectangular dot pattern demonstrates that the crystal is phase locked to the rotating field that is ($f_E = f_{RW}$).

Here the rotating wall electric field changes the trap potential in the

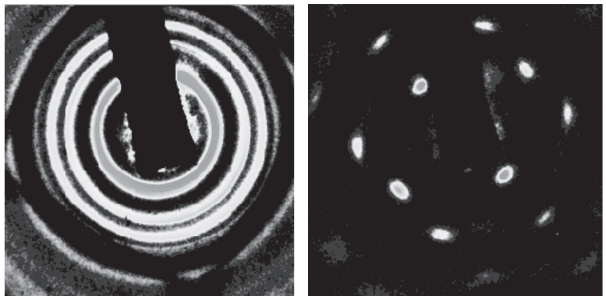

Fig. 7. a) Time averaged diffraction pattern and b) strobed diffraction pattern.

rotating frame, the plasma boundary is slightly deformed to a try-axial ellipsoid, and the shear force in the crystal transmit the torque to the interior. The plasma shape deformation has been measured and is typically less than 1%, but it generates a sufficient torques to phase lock the plasma rotation.

The NIST group demonstrated the rotating wall technique works in the strongly coupled regime, and that the plasma rotation is phased lock to the rotating wall drive for long period of time.

Rotating Wall Summary

The rotating wall is a very successful technique, allowing essentially unlimited confinement of non-neutral plasmas. The frequency of the rotating wall controls the plasma density. The coupling of the rotating perturbation to the plasma is well understood for crystallized plasma, but in the "plasma" regime many plasma distortions (such as waves) can contribute.

3. Centrifugal Separation

The bulk rotation of a multi-species ion plasma tends to produce centrifugal separation of its component species. To understand the mechanism, let's write the radial force balance of a small piece of plasma located at radius r.

$$0 = n_a(r)[qE(r) - qB\omega_{ra}r + m\omega_{ra}^2 r] - \frac{\partial p_a}{\partial r} \tag{20}$$

where $p_a = n_a k_B T_a$ is the thermal pressure of species a. With $B > 0$ and $\boldsymbol{B} = -B\hat{z}$ here, all frequencies (ω_{ra}, ω_E) are positive and $\omega_r \equiv \dot{\theta}$. [Other

conventions chose $\boldsymbol{B} = B\hat{z}$, and define a "*rotation frequency*" $\tilde{\omega}_r \equiv -\dot{\theta}$ so as to make $\tilde{\omega}_r > 0$].

Equation 20 can be rewritten in terms of rotation ω_E and cyclotron Ω_{ca}"frequencies":

$$\omega_E(r) = \frac{E(r)}{Br} \quad \text{and} \quad \Omega_{ca} = \frac{qB}{m_a} \tag{21}$$

giving:

$$\omega_{ra} = \omega_E(r) - \frac{1}{qBn_a(r)r}\frac{\partial p_a}{\partial r} + \frac{\omega_{ra}^2}{\Omega_{ca}} \; . \tag{22}$$

The last term is the centrifugal correction to the rotation rate; is generally small but it causes centrifugal separation. Before reaching thermal equilibrium, each species rotates at a different rate, and the collisional drag between species causes torques which drive one species out and the other in. Consider a drag force for species a of the form

$$F_{\theta a} = -\sum_b \nu_{ab}\; m_a r(\omega_{ra} - \omega_{rb}) \tag{23}$$

where ν_{ab} is the collision rate between species a and b. This drag θ-force produces a $F_\theta \times B$ drift in the radial direction that causes centrifugal separation. The resulting radial flux Γ_{ra} of species a is simply the charge density times the drift velocity. Combining the last two equations one gets:

$$\Gamma_{ra} = n_q \frac{F_{\theta a}}{qB} = \sum_b \frac{D_{ab}}{k_B T_a}\left[\frac{\partial p_a}{\partial r} - \frac{n_a}{n_b}\frac{\partial p_b}{\partial r} + n_a(m_b\omega_{rb}^2 - m_a\omega_{ra}^2)r\right] \tag{24}$$

where $D_{ab} = \nu_{ab}\; r_{ca}^2$ is a diffusion coefficient and $r_{ca} = \sqrt{k_B T_a}/\Omega_{ca}$ is the thermal cyclotron radius of species a. The first two terms are diffusive fluxes, which tend to mix the species, while the last term is a mobility term separating the species due to centrifugal force acting on each species. Note that the flux Γ_{ra} vanishes when $T_a(r) = T_b(r) = T$, $\omega_{ra}(r) = \omega_{rb}(r) = \omega_r$ and the densities satisfy thermal equilibrium.

In thermal equilibrium, each species density can be written as:[3]

$$n_a(r) = n_a(0)\exp\left[\frac{-q_a}{k_B T}\left(\phi(r) - \frac{m_a}{q_a}\frac{\omega_r^2 r^2}{2} - \frac{B\omega_r r^2}{2}\right)\right] \tag{25}$$

Note that the only difference between species comes from the ω_r^2 term, and for the separation to be significant, this term must be large compared to

the thermal energy $k_B T$. More precisely for simple two species case, the following has to be satisfied:

$$q\left|\frac{m_1}{q_1}-\frac{m_2}{q_2}\right|\omega_r^2 R_p^2 > k_B T \tag{26}$$

The separation length is defined as :

$$l_{sep} \equiv \frac{k_B T}{|m_1 - m_2|\,\omega_r^2 R_p}\ . \tag{27}$$

When $l_{sep} < R_p$ separation occurs in the plasma, and when $l_{sep} \ll \lambda_D$ then complete separation takes place, with species arranged in separate concentric rings.

For two species carrying the same charge, equation 25 leads to:

$$\frac{n_a(r)}{n_b(r)} = C_{ab}\exp\left[\frac{1}{2k_B T}(m_a - m_b)\,\omega_r^2 r^2\right] \tag{28}$$

where C_{ab} is a constant determined by the overall fraction of each species.

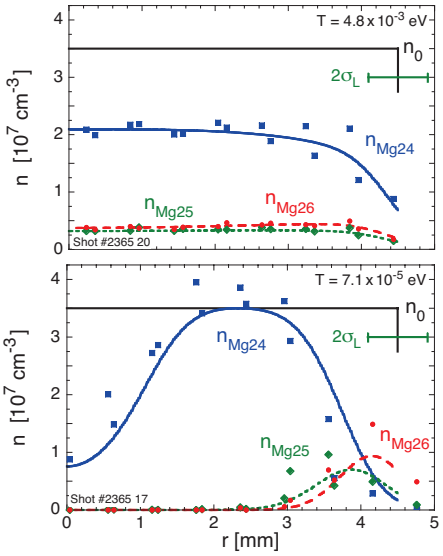

Fig. 8. Radial density profile of multi-species plasma showing warm un-separated plasma (top), and cold separated plasma (bottom).

Shown on figure 8 are measured density profiles for a warm plasma with negligible separation (top), and for a cold plasma with strong separation[12] (bottom). The symbols represent LIF-measured densities of magnesium

ion isotopes. The solid flat line is the total density n_0 obtained from the rotation frequency. The curves are predictions of equation 28, here the theory prediction have been convoluted with the finite size probe laser beam σ_l so they can be compared directly with the experimental measurements. At $T = 4.8 \times 10^{-3}$ eV, the species are uniformly mixed. Note that the sum of the Mg^+ isotopes is 25% lower than to the total plasma density due to the presence of impurity ions H_3O^+ and O_2^+ not detected by the LIF diagnostic. As the plasma is laser cooled down to $T = 7.1 \times 10^{-5}$ eV, the species centrifugally separate and concentrate into radial annuli. The central hole observed in the Mg^+ density is the result of the lighter impurity species H_3O^+.

More dramatic separation is routinely observed in electron-antiproton plasmas.[13]

The rate $\mathcal{R}$ at which the centrifugal separation occurs can be easily estimated if the mobility flux is smaller or equal to the diffusive flux. This rate is then roughly the rate required for particles to diffuse across the plasma radius r_p.

$$\mathcal{R} \sim \frac{D_{ab}}{r_p^2} \sim 0.1 s^{-1} \left(\frac{n_0}{10^7 cm^{-3}}\right) \sqrt{\frac{\mu(amu)}{T}} \left(\frac{1}{B(Tesla) R_p(cm)}\right)^2 \quad (29)$$

Shown on figure 9 is the re-mixing rate of previously separated magnesium ions isotopes. The plasma is abruptly heated with a burst of cyclotron heating, changing from $T \sim 5 \times 10^{-5}$eV to $T \sim 10^{-3}$ eV. The squares are LIF measurements of the normalized density ratio Mg_{25}/Mg_{24}. The solid line is the result of a calculation of the flux Γ_{ra} from equation 24 starting from the initially measured density profiles and measured $T(t)$.

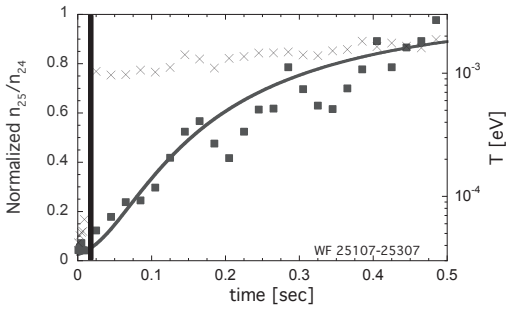

Fig. 9. Re-mixing of magnesium isotopes after a burst of heat (black vertical bar). × represents temperature and squares are concentration of Mg_{25}.

Centrifugal Separation Summary

We have seen that multi-species plasma are centrifugally separated when the centrifugal energy is larger than the thermal energy (Eq. 26) and that the separation is complete when the separation length is smaller than the Debye screening length (Eq. 27). For plasma close to thermal equilibrium: the radial densities distribution and the separation-remixing rate are correctly describe by a drag force due to collision between species.

4. Simple Tutorial Problems

4.1. *Problem 1*

Calculate the $\boldsymbol{E}\times\boldsymbol{B}$ rotation frequency of a single species, uniform plasma, of density 10^7cm^{-3} in a 3 Tesla magnetic field.
a) Consider an electron plasma.
b) Consider a Magnesium ion plasma.

As we have seen in the first section of this chapter, $\boldsymbol{E}\times\boldsymbol{B}$ rotation rate of a constant density plasma is:

$$f_E = \frac{nq}{4\pi\epsilon_0 B} \cong \frac{10^{13}\cdot 1.6\times 10^{-19}}{4\pi\cdot 8.8\times 10^{-12}\cdot 3} \cong 4.8\text{kHz}$$

Note that here we are assuming that the density is low compare to the maximum density achievable in a Penning trap ("*Brillouin density*"). For most plasmas in Penning traps this assumption is satisfied (i.e. $2\omega_r \ll \Omega_c$). Here the cyclotron frequency of a singly ionized magnesium ion is $\Omega_c^{Mg_{24}}/2\pi \cong 1.9\text{MHz}$, clearly within our approximation. For plasmas approaching the Brillouin limit, a rigorous description is given by D. Dubin in the chapter on plasmas in Penning trap.

$E\times B$ drifts are independent of the mass of the trapped charged particles, but dependent on the charge q. Therefore ions and electrons rotate in opposite direction. Figure 1 of this chapter shows the (positive) rotation direction for positive charges in $\boldsymbol{B} = -B\hat{z}$.

4.2. *Problem 2*

Estimate the minimum rotation frequency necessary to observe centrifugal separation of magnesium 24 from magnesium 25 for a temperature of 10K and a plasma radius of 5mm.

Assuming thermal equilibrium we have see that for singly ionized ion the separation occurs when:

$$|m_1 - m_2| \, (2\pi f_E R_p)^2 > k_B T$$

Therefore

$$\begin{aligned} f_E &> \frac{1}{2\pi R_p} \sqrt{\frac{k_B T}{|m_1 - m_2|}} \\ &> \frac{1}{2\pi \cdot 5 \times 10^{-3}} \sqrt{\frac{1.38 \times 10^{-23} \cdot 10}{|\,25 - 24\,| \cdot 1.67 \times 10^{-27}}} \\ &> 9.15\text{kHz} \end{aligned}$$

Acknowledgements

This work was supported by National Science Foundation Grant PHY-1414570, Department of Energy Grant DE-SC0002451and Department of Energy High Energy Density Laboratory Plasma Grant DE-SC0008693. The author thanks the organizers of Les Houches Winter School for the opportunity to contribute to the workshop. The author also thanks Prof. C.F. Driscoll, Prof. D.H.E. Dubin and Prof. T.M.O'Neil for many years of enlightening guidance and theoretical support.

References

1. T.M. O'Neil, A Confinement Theorem for Nonneutral Plasmas, *Phys. Fluids* **23**, 2216-2218 (1980). D.H.E. Dubin and T.M. O'Neil, Trapped Nonneutral Plasmas, Liquids, and Crystals (The Thermal Equilibrium States), *Rev. Mod. Phys.* **71**, 87-172, (1999).
2. D.J. Heinzen, J.J. Bollinger, F.L. Moore, W.M. Itano, and D.J. Wineland, Rotational Equilibria and Low-Order Modes of a Non-Neutral Ion Plasma, *Phys. Rev. Lett.* **66** , 2080-2083 (1991).
3. T.M. O'Neil and D.H.E. Dubin, Thermal Equilibria and Thermodynamics of Trapped Plasmas with a Single Sign of Charge, *Phys. Plasmas* **5**, 2163-2193, (1998).
4. T.M. O'Neil, Cooling of a Pure Electron Plasma by Cyclotron Radiation, *Phys. Fluids* **23**, 725 (1980).
5. B.R. Beck, J. Fajans, and J.H. Malmberg Temperature and Anisotropic-Temperature Relaxation Measurements in Cold, Pure-Electron Plasmas, *Phys. Plasmas* **3**, 1250 (1996).
6. J. R. Danielson, D. H. E. Dubin, R. G. Greaves and C. M. Surko, Plasma and Trap-Based Techniques for Science with Positrons, *Rev. Mod. Phys.*, **87**, 247 (2015).

7. D.J. Larson, J.C. Bergquist, J.J. Bollinger, W.M. Itano, and D.J. Wineland, Sympathetic Cooling of Trapped Ions: A Laser Cooled Two Species Nonneutral Ion Plasma, *Phys. Rev. Lett.* **57**, 70-73 (1986).
8. G. Gabrielse, X. Fei, L.A. Orozco, R.L. Tjoelker, J. Haas, H. Kalinowsky, T. Trainor, W. Kells, Cooling and Slowing of Trapped Antiprotons Below 100 meV, *Phys. Rev. Lett.* **63**, 1360-1363 (1989).
9. X.-P. Huang, F. Anderegg, E.M. Hollmann, C.F. Driscoll and T.M. O'Neil, Steady-State Confinement of Non-neutral Plasma by Rotating Electric Fields, *Phys. Rev. Lett.* **78**, 875-878 (1997). F. Anderegg, E.M. Hollmann, and C.F. Driscoll, Rotating Field Confinement of Pure Electron Plasmas Using Trivelpiece-Gould Modes, *Phys. Rev. Lett.* **78**, 4875 (1998).
10. J. R. Danielson, C. M. Surko and T. M. O'Neil, High-density Fixed point for Radially Compressed Single-component Plasmas, *Phys. Rev. Lett.* **99**, 135005, (2007).
11. X.-P. Huang, J.J. Bollinger, T.B. Mitchell, W.M. Itano, and D.H.E. Dubin, Precise control of the global rotation of strongly coupled ion plasmas in a Penning trap, *Phys. Plasmas* **5**, 1656 (1998).
12. M. Affolter, F. Anderegg, D. H. E. Dubin, and C. F. Driscoll, Cyclotron Mode Frequency Shifts in Multi-Species Ion Plasmas, *Physics of Plasmas* **22**, 055701, (2015).
13. G.B. Andresen, et al., Centrifugal Separation and Equilibration Dynamics in an Electron-Antiproton Plasma, *Phys. Rev. Lett.*, **106** 145001, (2011).